Porous carbon spheres from poly(4-ethylstyrene-co-divinylbenzene): role of ZnCl2 and KOH agents in affecting porosity, surface area and mechanical properties

UNIVERSITÀ DEGLI STUDI DI TORINO

Microporous and Mesoporous Materials

Volume 288, 1 November 2019, art. n. 109605

DOI: 10.1016/j.micromeso.2019.109605

Porous carbon spheres from poly(4-ethylstyrene-co-divinylbenzene), role of ZnCl2 and KOH agents in affecting porosity, surface area and mechanical properties

Federico Cesano[1§], Sara Cravanzola[1§*], Valentina Brunella[1], Domenica Scarano[1*]

[1] Department of Chemistry, NIS (Nanostructured Interfaces and Surfaces) Interdepartmental Centre and INSTM Centro di Riferimento, University of Torino, Via P. Giuria, 7, 10125 Torino, Italy.

[§] Both authors contributed equally to this work.

* Corresponding authors: sara.cravanzola@unito.it, domenica.scarano@unito.it

Keywords

Carbon spheres, activated carbons, $ZnCl_2$, KOH, microporosity, mesoporosity, microindentation, scanning electron microscopy, atomic force microscopy, X-ray diffraction.

Abstract

The synthesis of activated-porous carbon spheres, from a cross-linked polystyrene copolymer alone and in presence of different activating agents, such as $ZnCl_2$ and/or KOH under thermal treatment at 800°C, is reported. In this paper, the role of both the $ZnCl_2$ and KOH not only as activating agents, but also as a hard template, is highlighted, which in addition avoid the collapse of the polymer spheres structure during the pyrolysis. It has been found that, while KOH favours the development of the microporosity and of the surface area, $ZnCl_2$ promotes the mesoporous character of the carbon spheres.

The focus of this work lies in the study of the effects of the combined use of $ZnCl_2$ and KOH. The simultaneous presence of the two activating agents led to a general increment of the mesoporosity, even if the surface area resulted to be higher than that obtained via $ZnCl_2$ alone activation and lower than in case of KOH alone. Structure, surface porosity and morphological properties of the samples have been characterized by X-ray diffraction, N_2-physisorption, scanning electron and atomic force microscopies. As the spherical shape is associated to high performances, from the mechanical point of view, and being structural integrity a strategic factor for applications, the elastic modulus and the hardness of a selection of samples have been determined. The evaluation of the mechanical properties by nanoindentation, rarely used in this context for this kind of systems, was found to be crucial for

foreseeing industrial applications and as an effective approach able to deal with micro-sized spheres and a relationship between surface area, porosity and mechanical properties has been discussed.

1. Introduction

Carbon materials have attracted much scientific attention, because of their outstanding properties. Due to their high surface area, porosity, electron conductivity and mechanical, thermal and chemical stability, activated porous carbons play an important role in several applications [1], including energy storage [2], catalysis [3], adsorption [4, 5] and purification from pollutants [6]. In these perspectives, one of the most relevant properties of such carbon-based materials is by far the porosity. For these reasons, the control of synthesis and process parameters is peculiar, in such a way to tailor and control the pore size and surface properties. In this regard, porous carbon materials have been synthesized over the years via carbonization at high temperatures of synthetic or natural precursors [7], using many different methods (i.e. activation by means of organometallic compounds and metal salts, physical activation, carbonization of polymer aerogels or blends) [8]. Evidently, the choice of the carbon precursor for pyrolysis is crucial. It is known that microporous carbons can be obtained by means of carbonization and subsequent activation of lignocellulosic materials [9] or waste-derived biomass [10, 11], from a mix of coal, phenol and formaldehyde precursors [12], furfuryl alcohol [13-15] or from spherical polystyrene based resins [16], or, in general, from polymers [17] or waste polymers [18]. Generally, the synthesis of activated porous carbons involves two steps. The first one is the pyrolysis of the selected precursor in a 300-900°C range temperature, during which the removal of the most non-carbon hetero-elements takes place. The second one is the activation step, which aims to develop the porosity and the surface area of the final carbon structure [19]. In this regard, it is well-known that, especially in the case of adsorption applications, the porosity of such carbon material plays a key role, where distinguishing between larger mesopores and/or micropores can be crucial [20].

For these reasons, being the uniformity of pores an outstanding objective, templating routes have paved the way to use hard templates during the pyrolysis of the selected precursor (i.e. like zeolites, clays, silicas and colloid crystals, cross-linked porous polymers) [21-24]. Whereas, in case of use of the so-called soft templates, the self-assembly of molecules is involved, able to retain the porosity upon a thermal treatment [25].

For the synthesis of porous carbons with high surface area, among the chemical activators, many reactants can be used, from mineral acids such as H_3PO_4, H_2SO_4 [26], strong bases (KOH and NaOH) [27, 28], or salts ($ZnCl_2$) (i.e. Lewis acids) [29]. Among them, KOH takes many advantages if compared to acids, from the costs and the low corrosion property points of view and results in a

defined micropore size distribution and high surface area [5, 30, 31]. Furthermore, the effect of the activation step that is responsible for the formation of porosity, in turn may increase or reduce (i.e. excessive activation) the surface area/pore volume, depending on several aspects, including activation agent type and quantity, nature of the carbon precursor, activation parameters (temperature, time, etc.). It was shown that, depending on the different activation mechanism, KOH produces usually the widening of micropores, whereas $ZnCl_2$ additionally develops small mesoporous in structure and H_3PO_4 leads to a more heterogeneous pore size distribution [15, 32-35]. Moreover, it is worth noticing that $ZnCl_2$ molecularly dispersed into a polymer resin, involves a series of processes and reactions (i.e. melting, vaporization, decomposition, oxidation, and reduction) occurring during the thermal treatment [15, 36], can be used as templating agents as well, in such a way to avoid the contraction of the material during the carbonization/activation step of the synthesis procedure [36].

Besides all these considerations, the appropriate shape and the hardness of the porous carbon materials are strategic factors for practical applications. In particular, spherical activated carbons [37-39] have attracted a huge interest in the industrial and research communities [40] because of their good adsorption properties, good liquidity, smooth surface, tunable porosity, controllable size distribution and excellent mechanical strength [41, 42]. The mechanical behavior of such micro and nanospheres play a key role in affecting the structural integrity of the final devices in which they are applied [43]. However, the control of the porosity and size of the carbon spheres is still challenging [5].

Considering all these aspects, in this work, the effects of different agents on the activation and carbonization processes of polymer waste spheres have been studied [18, 44, 45]. Specifically, different porous carbon spheres have been synthesized from the carbonization of polystyrene-co-divinylbenzene (PS-co-DVB) by the combined activation with $ZnCl_2$ and/or KOH taking also advantage of the hard-templating role of the $ZnCl_2$ salt. PS-co-DVB was selected to take advantages from its crosslinked and porous nature, and together with its peculiar spherical shape [46, 47]. The structure and the surface properties of the so-obtained spheres have been investigated by means of a multi-technique approach based on X-ray diffraction (XRD), scanning electron microscopy (SEM), atomic force microscopy (AFM) and N_2 physisorption using Brunauer-Emmett-Teller method (BET) for the determination of the surface area.

As KOH and $ZnCl_2$ are the common activating agents used to obtain different porosity properties, the results of their combined use have been analyzed and compared to those obtained from the single use of KOH or $ZnCl_2$. Moreover, the mechanical properties of the porous carbon spheres have been studied by means of microindentation, thus evaluating how the surface porosity properties could

affect the mechanical properties of the spheres. Furthermore, the indentation method that is very rarely used for microspheres, has been verified to test the material for reliable and industrial applications.

2. Materials and methods

2.1 Synthesis

Poly(4-ethylstyrene-co-divinylbenzene) (1g, *hereafter PS-co-DVB*) pure crosslinked polymer microspheres (Scheme 1, *Step a*), PS-co-DVB microspheres containing $ZnCl_2$ (Scheme 1, *Step b1*) or KOH (Scheme 1, *Step b2*) as activating agents, was thermally treated up to 800°C under N_2 gas flow. Pure KOH were mixed to the copolymer in the 1:3 weight ratio, whereas $ZnCl_2$ dissolved in hot ethanol (110°C, 10 ml) and then mixed (1:3:3 or 1:10:3 weight ratios of copolymer, $ZnCl_2$ and ethanol, *hereafter $ZnCl_2$ 1:3* or *$ZnCl_2$ 1:10*), stirred and thermal treated at 80°C for 24h. Then, the $ZnCl_2$-activated carbon microspheres (in the 1:10 weight ratio) were mixed with KOH (carbon:KOH 1:5 w/w) and treated again at 800°C in N_2 gas flow (Scheme 1, *Step b1.2*). After the thermal treatment, the two samples activated by KOH were diluted with 3M HCl solution and finally washed with distilled water.

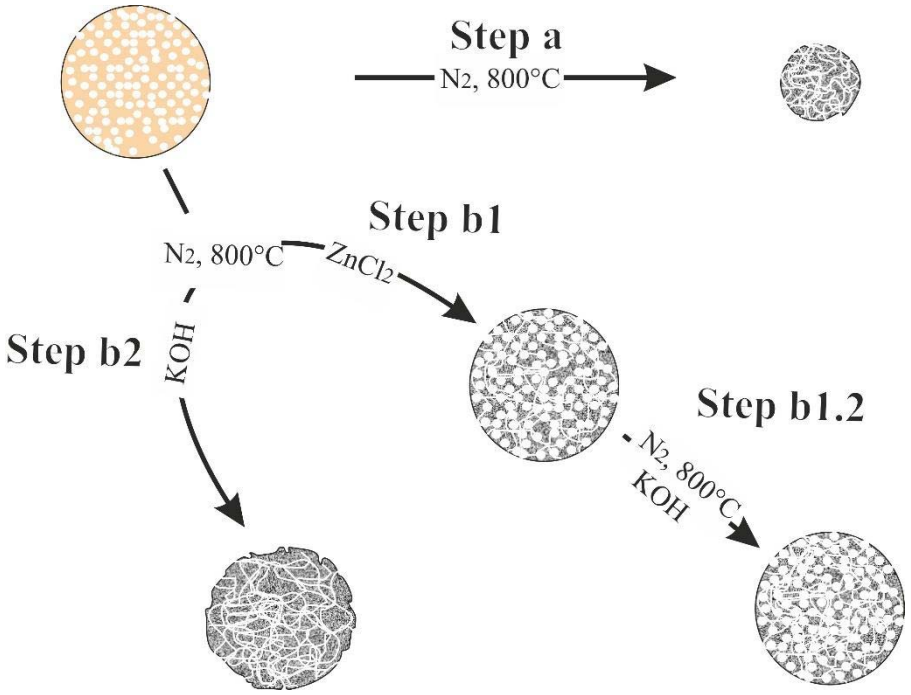

Scheme 1. Carbon microspheres preparation steps, during the thermal treatment (800°C, N_2) from pure PS-co-DVB (*step a*) and with different activating agents, KOH (*step b2*), or $ZnCl_2$ (*step b1*) and subsequent thermal treatment with KOH (*step b1.2*)

2.2 Characterization

Samples were investigated at different preparation steps. The microsphere morphology and structure were investigated by means of scanning electron microscopy (SEM, Zeiss Evo 50 SEM instrument operating at 30 kV) and atomic force microscopy (AFM, Nanosurf Easyscan2 AFM instrument, equipped with a 10x10μm scan-head, an enclosure acoustically insulated and an antivibration platform), with 1x1 μm scanning acquisitions in the intermittent contact mode. Phase structure of the spheres was attained by X-ray diffraction (XRD) analysis (PAN-analytical X' Pert PRO diffractometer) equipped with a metal copper source, in a Bragg–Brentano geometry. The identification of the phases was attained by comparing XRD patterns with the powder diffraction file (PDF) reference of the International Centre for Diffraction Data (ICDD).

To determine the porous texture of materials at the different steps of the preparation, N_2-adsorption/desorption isotherms were obtained at 77K, by means of Micromeritics ASAP 2020 instrument. Before analysis, samples were outgassed either at RT overnight (PS-co-DVB) or at 400°C (carbon materials resulting from the activation treatments). The surface area (S_{BET}) values were calculated from the *Brunauer–Emmett–Teller* (BET) equation (0.05–0.25 p/p_0 as pressure range), while total pore volumes (V_{tot}) were calculated from the amount of nitrogen adsorbed at 0.98 p/p_0. Micropore surface area (S_{micro}) and volume (V_{micro}) were calculated from N_2-adsorption isotherms (Carbon Black STSA *t-plot* equation), while mesopore volume values were calculated from $V_{meso} = V_{tot} - V_{micro}$. Pore size distributions (PSDs) were attained by using a non-negative least squares fitting on the N_2-adsorption isotherms by applying the Density Functional Theory (DFT) method (slit-geometry DFT-model). Microindentation tests were performed on single particles by means of a microindenter Fischerscope HM2000, Microhardness Measurement System with WIN-HCU Software, and the elastic modulus and Vickers hardness have been calculated. All indentation measurements were performed in air at room temperature and the spheres were partially embedded in a polymer resin to fix them to a glass support. An increasing load of 2000 mN/20 sec for $ZnCl_2$/PS-co-DVB sample and 800 mN/20 sec for PS-co-DVB was applied, while the load decrease was 0.400 mN/20 sec for both of them. The mean values of Young's modulus and Vickers hardness (HV) were derived from load vs. indentation curves. Ten indentation measurements were performed for each sample.

3. Results and discussion

3.1 Structure, morphology and porosity properties

The crystalline structure of the microsphere, at each preparation step, was investigated by XRD and the obtained results are illustrated in Figure 1.

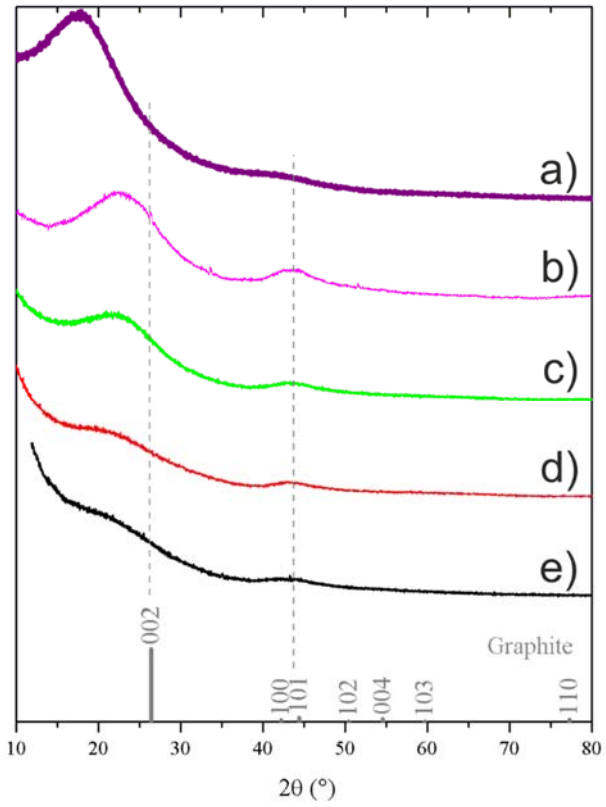

Figure 1. X-ray diffraction patterns of: a) PS-co-DVB spheres, b) PS-co-DVB pyrolyzed at 800°C, c) PS-co-DVB spheres activated with $ZnCl_2$ (1:10) and thermally treated at 800°C, d) $ZnCl_2$/KOH activated PS-co-DVB after thermal treatment at 800°, e) PS-co-DVB after the thermal activation at 800°C in presence of KOH. Graphite XRD peak positions are shown as reference material at the bottom of the graph.

XRD pattern of the cross-linked polystyrene copolymer (pattern a) exhibits a broad feature in the 2θ = 10°-30° interval due to the amorphous structure of the polymeric scaffold [48], whose maximum at about 2θ = 18° shifts to higher values (2θ ~ 25°) after the treatment at 800°C (pattern b) and can be ascribed to the (002) XRD features of carbon in the graphitic structure. Besides, the less intense and very broad feature, in the 2θ = 40°-50° range, can be ascribed to a sort of convolution band of the (100) with (101) XRD diffraction planes of the graphite, named as the (10) band. All the mentioned features appear very broad, underlying the not well organized and amorphous character of the samples [46]. It is also worth noticing that Zn species are absent, due to their degradation/vaporization nature and to the carbon, which acts as a reducing agent during the thermal treatments at 800°C [15, 36]. Moving to the patterns of the carbons obtained in presence of different activating agents, from $ZnCl_2$ 1:3 (see Figure S1, Supplementary Material), to $ZnCl_2$ 1:10 (Figure 1, pattern c), $ZnCl_2$/KOH (Figure

1, pattern d) and then to KOH, (Figure 1, pattern e), it can be observed that the diffraction features related to (002) and to (10) diffraction planes of the graphite become broader and low in intensity, especially when KOH combined to $ZnCl_2$ is used (pattern d) or, even more, in case of KOH alone (pattern e).

More in detail, notice that with a higher concentration of activating agents, moving from $ZnCl_2$ 1:3 to $ZnCl_2$ 1:10, the intensity of the graphite features is decreasing (Figure S1, Supplementary Material). Some more, the basic character of KOH causes an even more dramatic effect on the same diffraction features (Figure 1, patterns a and b).

This phenomenon is indicative of the significant role of the activating agent in affecting the crystallinity of the obtained carbons. On the other hand, after the thermal treatment at 800°C for 5h the presence of carbon with a small content of oxygen without zinc and potassium contributions can be detected by elemental analysis, thus evidencing that activating agents have a different chemical reactivity, affect in a different way the porosity, but they disappear from the final structure under the adopted conditions.

Low-magnification SEM images, representative of samples at the different preparation steps are illustrated in Figure 2a-e.

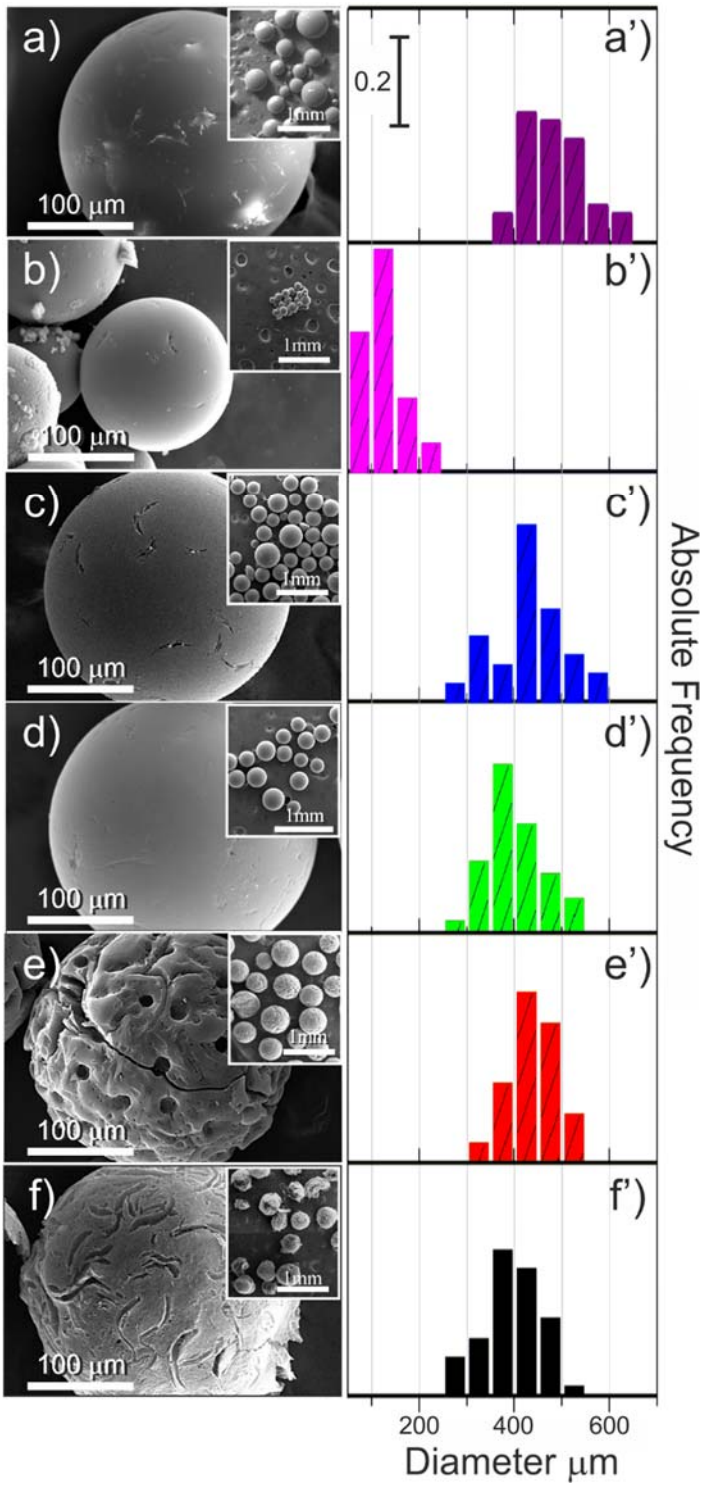

Figure 2. SEM images (left panels with insets) and sphere size distributions (right panels) at different steps of preparation of: a,a') PS-co-DVB precursor; b,b') PS-co-DVB treated at 800°C; c,c') PS-co-DVB/$ZnCl_2$ 1:3 treated at 800°C; d,d') PS-co-DVB/$ZnCl_2$ 1:10 treated at 800°C e,e') PS-co-DVB/$ZnCl_2$/KOH treated at 800°C; f, f') PS-co-DVB/KOH thermally treated at 800°C.

From Figure 2 a, a' the typical spherical shape of PS-co-DVB particles is SEM imaged together with their size distribution. Notice that the particles preserve their typical shape during the treatment at

800°C, even though the dimensions of the spheres are noticeably decreased, from 400-600 μm range to 100-300 μm, because of sintering effects (Figure 2a, 2b), as well illustrated by the particle size distributions (Figure 2a', 2b'). The collapse of the sphere structure is totally avoided when $ZnCl_2$ is embedded in the polymer matrix, as shown in Figure 2c, 2c', 2d, 2d'. The shape of the obtained sample is still spherical, but the dimensions (~250-550 μm) are not so far from the original raw material. It is worth noticing that the $ZnCl_2$ concentration doesn't affect in a visible way the shape and size of the sample, as demonstrated by comparing Figure 2 c,c' and Figure 2 d, d', which compare samples obtained from PS-co-DVB/$ZnCl_2$ precursors treated at 800°C but containing different amount of $ZnCl_2$ (1:3 and 1:10 wt, respectively).

The same considerations can be made for the samples treated with KOH, in the presence or not of $ZnCl_2$ activating agent (Figure 2 d, d' and 2 e, e', respectively). As a matter of fact, in both cases, the shape and the size of the spheres are maintained, but the surface of the samples appears to be highly damaged, due to the presence of holes and cracks. In particular, $ZnCl_2$ does not seem to affect the surface roughness of the spheres, whereas KOH is responsible for the formation of deep and irregular cavities decorating the whole surface. Therefore, from these images, it is clear that both $ZnCl_2$ and KOH embedded in the PS-co-DVB polymer particles play an important role, during the thermal treatment occurring under N_2 atmosphere at 800°C, in preserving the structural shape and dimension of the raw sample. However, in order to investigate the local surface structure in a more detailed way, an investigation at higher magnification is needed.

To this purpose, high-resolution SEM/AFM sample images at the different preparation steps are illustrated in Figure 3.

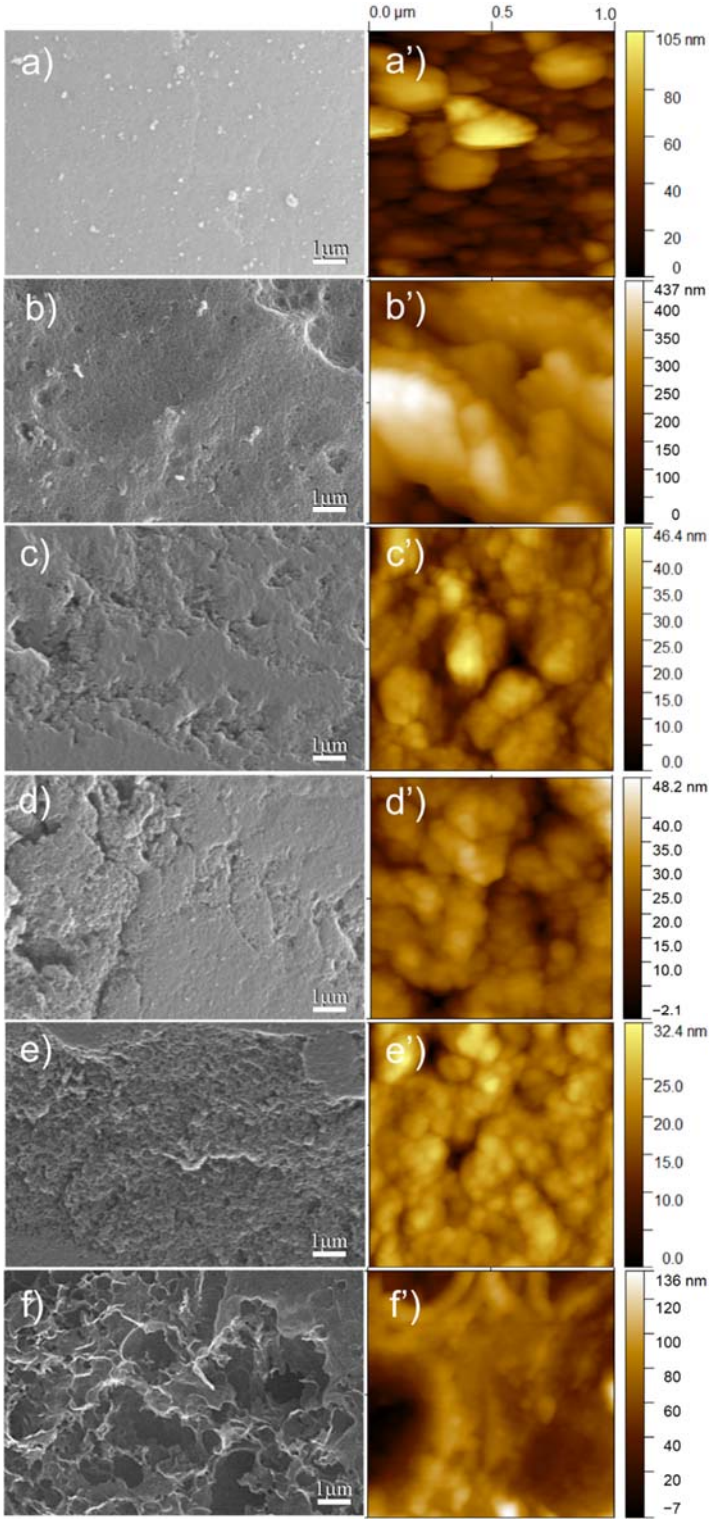

Figure 3. High resolution SEM (left panels) and AFM (right panels) images of: a,a') PS-co-DVB precursor; b,b') PS-co-DVB treated at 800°C; c,c') PS-co-DVB/$ZnCl_2$ 1:3 at 800°C; d,d') PS-co-DVB/$ZnCl_2$ 1:10 at 800°C; e,e') PS-co-DVB/$ZnCl_2$/KOH at 800°C; f,f') PS-co-DVB/KOH at 800°C.

The SEM image of the co-polymer, before thermal treatment (Figure 3a), shows a quite homogeneous and smooth surface, while a deeper investigation of its topography (see AFM image, Figure 3a') reveals the presence of particle aggregates ranging in the 0.1-0.4 μm size interval, whose rounded shapes are quite well defined. When the polymer previously treated at 800° C for 5 hours is considered (Figure 3b, b'), the SEM image highlights the formation of wrinkles and cracks, which characterize a rougher surface. From the AFM analysis, it can be also noticed that, together with a lower definition of the particle shape, the dimensions of the single domains are decreasing, while aggregation processes, due to sintering effects, are occurring. The spheres obtained by embedding $ZnCl_2$ at different concentrations, 1:3 and 1:10 wt, inside the PS-co-DVB copolymer, are shown in Figure 3c, c' and Figure 3 d,d', respectively. For both the samples, from SEM images, (Figure 3c, 3d) the surface appears to be quite flat, even if interrupted by some cracks. Conversely, moving to higher resolution AFM images (Figure 3c', d'), a defective surface, with small domains and nanoparticles about 0.1 μm in diameter, responsible for the higher porosity and surface area, can be highlighted (as demonstrated by BET analysis, *vide infra*).

Moreover, when the sample obtained from PS-co-DVB/$ZnCl_2$, then treated with KOH, is considered, the increase in the surface roughness is already clearly detectable by SEM investigation (Figure 3e), while the presence of small nanoparticles and grains is again confirmed by the AFM image (Figure 3e').

Finally, considering the PS-co-DVB spheres treated with KOH (Figure 3 f, f'), the effects of the treatment in KOH alone are even more evident, already at low resolution, thus highlighting the formation of a fragmented and highly porous surface. The effects due to the strength of the treatment with KOH are even clearer from the AFM image that shows a completely irregular surface morphology, with deep hollows and high roughness, which predicts a high porosity.

The N_2-adsorption/desorption isothermal curves and the associated pore size distributions, attained by applying the DFT (Density Functional Theory) method, of the porous spheres at the different steps of the synthesis are illustrated in Figure 4. Table 1 summarizes their BET surface area (S_{BET}), microporous (S_{micro}) and mesoporous (S_{meso}) surface area properties.

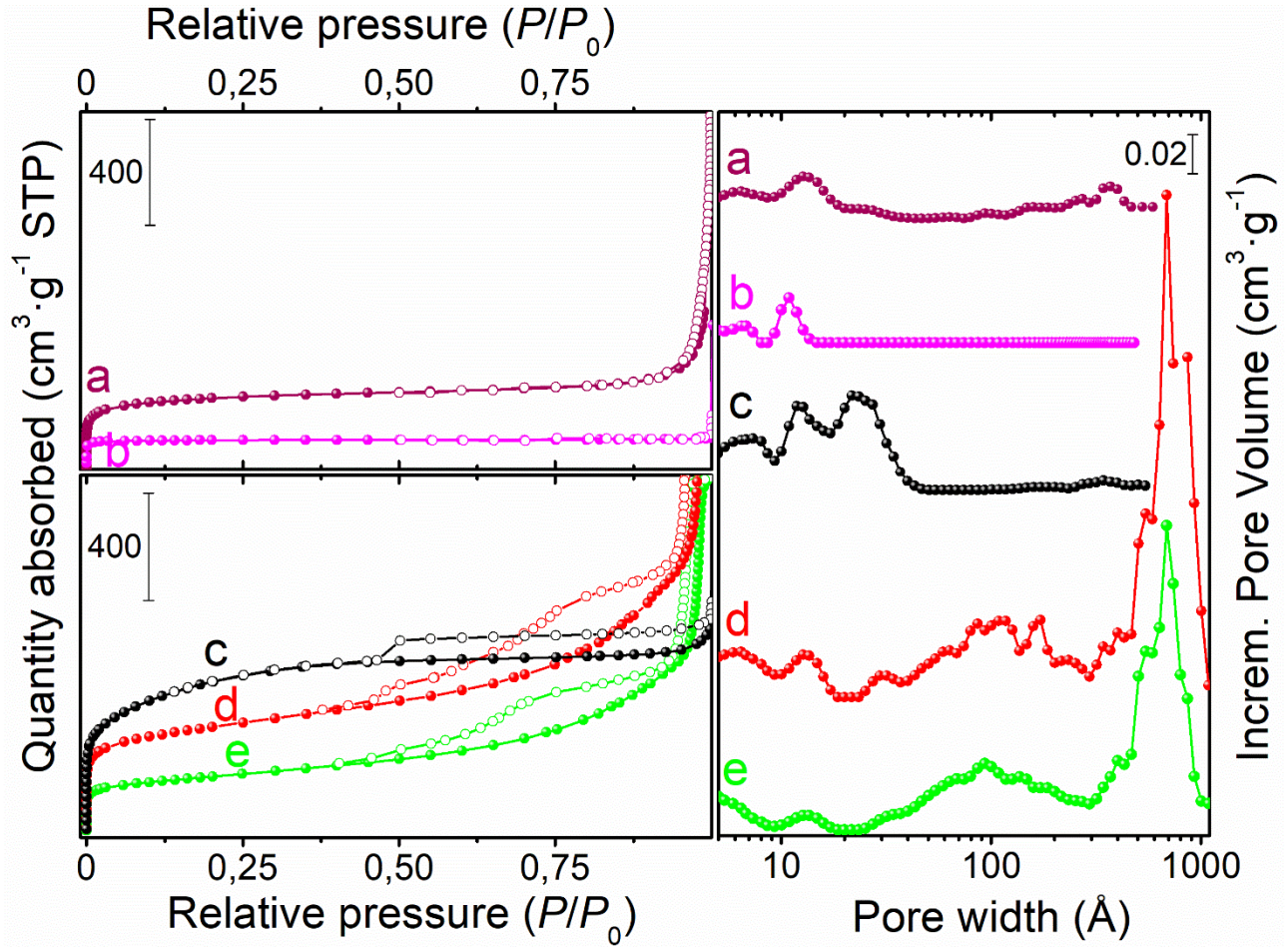

Figure 4. N_2 absorption/desorption isotherms (left panels) and PSDs (right panel) of PS-co-DVB as it is (a, purple curves), PS-co-DVB treated at 800°C (b, magenta curves), PS-co-DVB/KOH activated at 800°C (c, black curves), PS-co-DVB/$ZnCl_2$/KOH activated at 800°C (d, red curves) and PS-co-DVB/$ZnCl_2$ 1:10 activated at 800°C (e, green curves).

Table 1. Summary of the surface area and pore volume values. [a] Total area evaluated following the BET model in the standard $0.05 < P/P_0 < 0.25$ pressure range; [b] Total pore volume calculated as the volume of the liquid at $p/p_0 \sim 0.98$; [c] V_{micro} calculated by using t-plot method (Harkins and Jura or Carbon Black STSA thickness equations for PS-co-DVB or the thermally treated samples, respectively); [d] $V_{meso} = V_{tot} - V_{micro}$.

	S_{BET}[a]	$S_{Langmuir}$	V_{TOT}[b]	V_{micro}[c]	V_{meso}[d]	(%) V_{meso}
PS-co-DVB as it is	930	1239	0.7732	0.3859	0.3873	50
PS-co-DVB 800°C	(386)	489	0.1799	0.1727	0.007	4
PS-co-DVB/$ZnCl_2$ 1:10 800°C	807		1.7136	0.1591	1.5545	91

PS-co-DVB/$ZnCl_2$/KOH 800°C	1469	2.3854	0.3224	2.063	86
PS-co-DVB/KOH 800°C	2095	1.1377	0.9203	0.2174	19

A type-I isotherm with an extended slope, indicating an extensive micropore distribution together with bigger pores in the cross-linked polymer scaffold, is displayed for PS-co-DVB (purple curves). Notwithstanding a more rectangular shape, the PS-co-DVB thermally treated under N_2 at 800°C (magenta line) also presents a type-I isotherm. Moreover, the lower N_2 uptake as a result of the small dimensions of the micropores, is indicative also of the smaller volume developed, because of the collapse of the sphere structure during the thermal treatment, as also evidenced by the before discussed particle-size diameters (Figure 2 a, b').

On the other hand, $ZnCl_2$-activated sample with $ZnCl_2$ 1:3 (see Figure S2, Supplementary Material), and 1:10 with or without KOH (Figure 4, green and red curves, respectively), all exhibit a blend of type-IV and type-I isotherms with an abrupt capillary condensation from ~0.5 p/p_0, thus revealing both mesoporous and microporous characters. Notice the presence of hysteresis loops, whose shape can be described as a combination of type H1 and type H4, being the former more common for materials exhibiting a narrow range of uniform mesopores, while the latter, with a more noticeable N_2 uptake at low p/p_0, due to the presence of micropores and often typical of micro-mesoporous carbons. Notice also that $ZnCl_2$-activated sample ($ZnCl_2$ concentrations 1:10) and the same after KOH treatment (green and red isotherms in the left panel of Figure 4, respectively) have a very similar shape. The shifting towards higher uptake is an indication of the KOH action in the formation of new micro- and small mesopores. The situation is completely different for PS-co-DVB spheres treated only with KOH (black curves), where type-I (b) isotherm is found together with an H4 hysteresis loop, thus well illustrating a predominant microporous material having a distribution of micropores covering a relatively broad range in conjunction with narrow mesopores [49]. It is worth mentioning that from the isotherms shape observed for $ZnCl_2$-treated microspheres nearby the saturation pressure ($p/p_0 \cong 1$), the contribution of macropores can be undertaken.

All these considerations find good agreement with the analysis of the PSDs determined by means of the DFT model (right panel in Figure 4). More in detail, PS-co-DVB before (purple curve) and after (magenta curve) thermal treatment show two families of micropores (one < 7Å and a second one in the 10-14 Å range). Additionally, the presence of larger pores (>500Å in size) con be highlighted for the cross-linked polymer. $ZnCl_2$ activated samples both with or without KOH (red and green curves, respectively), show in addition to micropores, a wide distribution of mesopores (from 50 to several

hundreds of Å). Otherwise, the PSD of PS-co-DVB sample treated only with KOH (black curve) reveals an important contribution of micropores (<7 Å and 10-20 Å in size) together with a family of narrow mesopores (20-40 Å in size) and mainly a negligible contribution of large mesopores.

Further considerations can be made from the analysis of the results reported in Table 1. The purely microporous character (perfectly type-I isotherm) of the carbon obtained from the pyrolysis of the crosslinked polymer (negative C value) is more reliably closer to the $S_{Langmuir}$ value. Different is the situation for the other isotherms, all evidencing mixed characters, for which the S_{BET} values appear more adequate. It is clear that the thermal treatment caused a strong decrease of the surface area of the spheres, while $ZnCl_2$ works not only as an activating agent, but also as a hard template in avoiding the collapsing of the spheres during carbonization at 800°C, as testified by the increment of mesoporosity (see Table 1). While the treatment with both KOH and $ZnCl_2$ strongly increases the porosity but does not affect the distribution of pores, in absence of $ZnCl_2$ the surface area is further increased, but the mesoporosity is almost inhibited, with a prevalent contribution of micropores [19]. From the obtained results, it can be concluded that, KOH strongly helps in increasing the microporosity and then the surface area of the carbon spheres, whereas $ZnCl_2$ plays a key role in increasing the mesoporosity.

3.2 Mechanical properties as obtained by microindentation

In such a way to understand how porosity and surface area could affect the mechanical properties and, consequently, the structural integrity of the spheres, microindentation tests were performed on three representative samples: i) pristine PS-co-DVB spheres, ii) PS-co-DVB/$ZnCl_2$ 1:10, iii) PS-co-DVB/KOH. The aim was to obtain information at first on the initial status of the polymer, then on a system with an intermediate porosity degree after treatment at 800°C in presence of $ZnCl_2$ activating agent and, finally, on a high surface area sample with high porosity, as obtained from the KOH activating agent.

It is crucial to underline that the hardness and Young's modulus of PS-co-DVB/KOH spheres could not be tested due to the very fragile nature of the porous scaffold (i.e. high porosity) coming from the remarkable action of KOH treatment. Actually, as previously shown by N_2 physisorption tests (Figure 4 and Table 1) and microscopy images (Figures 2 and 3), the KOH activated carbon spheres broke even under very low loads (Figure S4 a, b, Supplementary Material). In fact the mechanical properties of sintered materials are reduced when the porosity increases [50]. Furthermore, also PS-co-DVB treated at 800°C was not tested because of the very small dimensions of the spheres (see Figure S4 c, Supplementary Material). For these reasons, only the results related to pristine PS-co-DVB spheres and PS-co-DVB/$ZnCl_2$ 1:10 are illustrated downwards. A scheme reporting the nanoindentation on a

sphere is reported in Figure 5a, while Figure 5b and 5c show the surface of PS-co-DVB/$ZnCl_2$ 1:10 before and after the indentation, respectively, where the sign of the diamond indenter is clearly visible.

Anyway, the results obtained are shown in Table 2 which lists the values of elastic modulus and hardness for each sample.

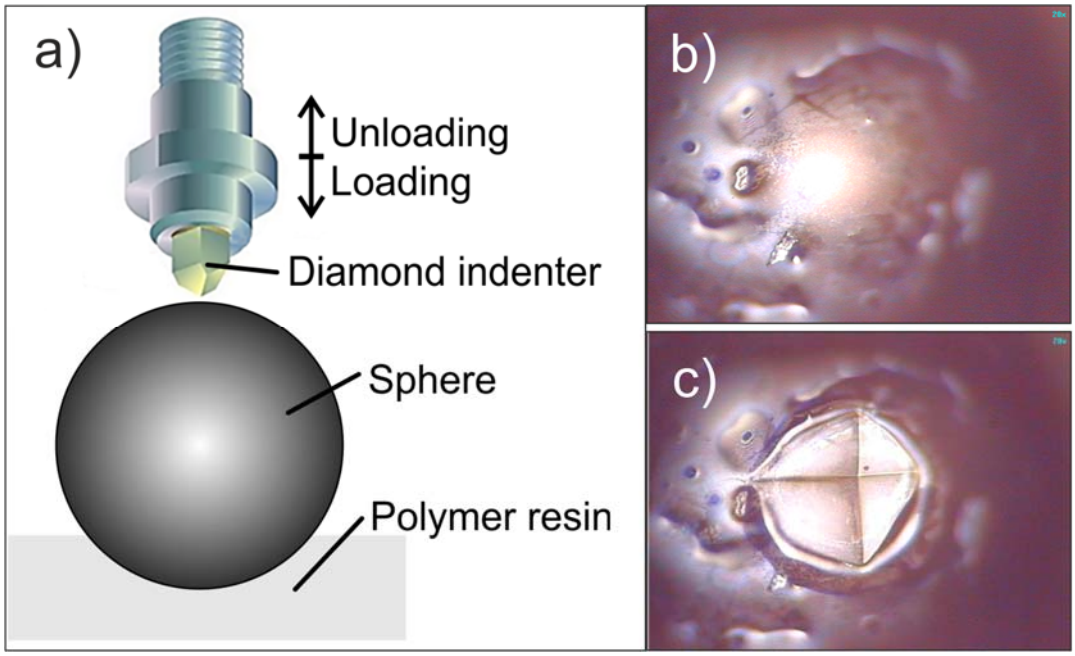

Figure 5. a) Scheme of an indentation test on a sphere partially embedded in a polymer resin; b) PS-co-DVB/$ZnCl_2$ sphere surface (20 x magnification) before the indentation and c) after the indentation test.

Table 2. Elastic modulus and Vickers Hardness for a selection of samples, as obtained by means of microindentation test.

	Elastic Modulus (GPa)	**Vickers Hardness (HV)**
PS-co-DVB	0.5 ± 0.1	2.3 ±1.2
PS-co-DVB/$ZnCl_2$ 1:10	3.3 ± 0.4	34 ± 5

First of all, it is worth noticing that the load applied for PS-co-DVB (800mN) is lower than that used for PS-co-DVB/$ZnCl_2$ 1:10 (2000mN), as it comes from the analysis of the force vs penetration depth graph shown in Figure S3 (Supplementary Material). In fact, when a loading of 2000 mN was imposed

on PS-co-DVB spheres, they were totally broken, as shown in Figure S4 a, b (Supplementary Material). This phenomenon can be considered as preliminary information concerning the mechanical behaviour of the pristine polymer spheres, being certainly more fragile than the sample treated at 800°C in presence of $ZnCl_2$.

Moreover, from the analysis of the data obtained from the microindentation tests shown in Figure 5a, elaborated and reported in Table 2, pristine PS-co-DVB manifests lower elastic modulus and Vickers Hardness values than those obtained on PS-co-DVB/$ZnCl_2$ 1:10, thus revealing a stiffer nature and a higher resistance to localized deformation after treatment at 800°C in $ZnCl_2$.

4. Conclusions

It is well known that KOH and $ZnCl_2$ play a relevant role in the activation of porous carbon materials. To this regard, we have prepared carbon spheres from the pyrolysis of wasted poly(4-ethylstyrene-co-divinylbenzene) precursor with the use of KOH or $ZnCl_2$ as activating agents, which led to the development of higher micro and mesoporosity, respectively, as expected. Remarkably, the effects of KOH or $ZnCl_2$ alone or combined during the pyrolysis step of the polymer at 800°C have been investigated by means of a multi-technique outline. While XRD analysis gave information concerning the structure of the carbon microspheres obtained from the different activating agents, SEM, AFM and N_2-physisorption revealed their morphology and porous texture. From this, it can be concluded that the simultaneous presence of KOH and $ZnCl_2$ can enhance both the micro- and mesoporosity of the so-obtained carbon spheres, while the surface area resulted to be higher than that obtained by using only $ZnCl_2$ (activating agent of small and extensive mesopores), but lower than obtained in the case of KOH alone (activating agent of micropores and narrow mesopores).

More remarkably, aiming at the correlation with the nature of the porous texture, a mechanical testing perfectly compatible with of the particles was developed. In this regard, the microindentation test on PS-co-DVB/KOH spheres was not possible. The spheres appeared to be very much fragile due to an excessive activation of the carbon structure well documented by microscopies. This phenomenon demonstrated that the treatment in pure KOH strongly degrades the mechanical properties and, hence, the structural integrity of the spheres, due to their strongly high porosity which causes the fragile nature of the sample. On the other hand, the results obtained on PS-co-DVB spheres and PS-co-DVB/$ZnCl_2$ in the 1:10 weight ratios show that the treatment at 800°C in the presence of $ZnCl_2$ as an activating agent can significantly improve the hardness and elastic modulus, showing the strong relationship between porosity, surface area and mechanical properties. On the basis of all the obtained data we can conclude that a compromise between the porosity and mechanical properties can be

found, due to the fact that an excessive activation can develop a higher porosity, but a lower mechanical resistance of the materials. However, it is possible to design suitable synthesis parameters (i.e. activating agent type, activation time and temperature) in such a way to better tailor all the properties of the final carbon spheres.

Interestingly, the presented activated carbon speres may find a relable use in industrial applications in the field of energy storage, adsorbent in liquid media and as catalyst supports in fixed or moving bed reactors, due to their porosity, mechanical hardness and packing property and chemical resistance.

Acknowledgments

This work was supported by MIUR (Ministero dell'Istruzione, dell'Università e della Ricerca), INSTM Consorzio and NIS (Nanostructured Interfaces and Surfaces) Inter-Departmental Centre of University of Torino.

Supplementary Material

Additional XRD patterns and N_2 physisorption isotherms of PS-co-DVB/$ZnCl_2$ samples are shown. Supplementary information and results concerning the microindentation tests have also been reported.

Author Contributions

The manuscript was written through contributions of all authors. All authors have given approval to the final version of the manuscript.

References

[1] M.R. Benzigar, S.N. Talapaneni, S. Joseph, K. Ramadass, G. Singh, J. Scaranto, U. Ravon, K. Al-Bahilyc, A. Vinu, Recent advances in functionalized micro and mesoporous carbon materials: synthesis and applications, Chem. Soc. Rev., 47 (2018) 2680.

[2] M. Sevilla, Energy storage applications of activated carbons: Supercapacitors and hydrogen storage, Energy Environ. Sci., 7 (2014) 1250.

[3] I. Matos, M. Bernardo, I. Fonseca, Porous carbon: A versatile material for catalysis, Catal. Today, 285 (2017) 194-203.

[4] H. Jin, Y.S. Lee, I. Hong, Hydrogen adsorption characteristics of activated carbon, Catal. Today, 120 (2007) 399-406.

[5] N.P. Wickramaratne, M. Jaroniec, Activated Carbon Spheres for CO_2 Adsorption ACS Appl. Mater. Interfaces, 5 (2013) 1849−1855.

[6] V. Bernal, L. Giraldo, J.C. Moreno-Piraján, M. Marco Balsamo, A. Erto, Mechanisms of Methylparaben Adsorption onto Activated Carbons: Removal Tests Supported by a Calorimetric Study of the Adsorbent–Adsorbate Interactions, Molecules, 24 (2019) 413.

[7] Y. Xia, Z. Yang, R. Mokaya, Templated nanoscale porous carbons, Nanoscale, 2 (2010) 639-659.

[8] J. Lee, J. Kim, T. Hyeon, Recent Progress in the Synthesis of Porous Carbon Materials, Adv. Mater., 18 (2006) 2073–2094.

[9] L. Zeng, X. Lou, J. Zhang, C. Wu, C. Jia, Carbonaceous mudstone and lignin-derived activated carbon and its application for supercapacitor electrode, Surf. Coat. Technol., 15 (2019) 580-586.

[10] R. Nisticò, F. Cesano, F. Franzoso, G. Magnacca, D. Scarano, I.G. Funes, L. Carlos, M.E. Parolo, From biowaste to magnet-responsive materials for water remediation from polycyclic aromatic hydrocarbons, Chemosphere, 202 (2018) 686-693.

[11] A.A. Arie, H. Kristianto, E. Demir, R. Demir Cakan, Activated porous carbons derived from the Indonesian snake fruit peel as anode materials for sodium ion batteries, Mater. Chem. Phys., 217 (2018) 254-261.

[12] H. Jiang, P. Desai, S. Kumar, A.S. Abhiraman, Carbon fibers from poly (p-phenylene benzobisthiazole) (pbzt) fibers: conversion and morphological aspects, Carbon, 29 (1991) 635-644.

[13] S. Bertarione, F. Bonino, F. Cesano, A. Damin, D. Scarano, A. Zecchina, Furfuryl Alcohol Polymerization in H−Y Confined Spaces: Reaction Mechanism and Structure of Carbocationic Intermediates, J. Phys. Chem. B, 112 (2008) 2580-2589.

[14] S. Bertarione, F. Bonino, F. Cesano, S. Jain, M. Zanetti, D. Scarano, A. Zecchina, Micro-FTIR and Micro-Raman Studies of a Carbon Film Prepared from Furfuryl Alcohol Polymerization, J. Phys. Chem. B, 113 (2009) 10571–10574.

[15] F. Cesano, D. Scarano, S. Bertarione, F. Bonino, A. Damin, S. Bordiga, C. Prestipino, C. Lamberti, A. Zecchina, Synthesis of ZnO-carbon composites and imprinted carbon by the pyrolysis of $ZnCl_2$-catalyzed furfuryl alcohol polymers, J. Photochem. Photobiol. A, 196 (2008) 143-153.

[16] H. Nakagawa, K. Watanabe, Y. Harada, K. Miura, Control of micropore formation in the carbonized ion exchange resin by utilizing pillar effect, Carbon, 37 (1999) 1455-1461.

[17] H.-M. Lee, D.-C. Chung, S.-C. Jung, K.-H. An, S.-J. Park, B.-J. Kim, A study on pore development mechanism of activated carbons from polymeric precursor: Effects of carbonization temperature and nano crystallite formation, Chem. Eng. J., In press (2019).

[18] F.G.F. de Paula, M.C.M. de Castro, P.F.R. Ortega, C. Blanco, R.L. Lavall, R. Santamaría, High value activated carbons from waste polystyrene foams, Microporous Mesoporous Mater., 267 (2018) 181-184.

[19] C.I. Contescu, S.P. Adhikari, N.C. Gallego, N.D. Evans, B.E. Biss, Activated Carbons Derived from High-Temperature Pyrolysis of Lignocellulosic Biomass, C, 4 (2018) 51.

[20] J. Qi, G. Wei, Y. Li, J. Li, X. Sun, J. Shen, W. Han, L. Wang, Porous carbon spheres for simultaneous removal of benzene and H_2S, Chem. Eng. J., 339 (2018) 499–508.

[21] B. Sakintuna, Y. Yurum, Templated Porous Carbons: A Review Article, Ind. Eng. Chem. Res., 44 (2005) 2893-2902.

[22] F. Cesano, D. Pellerej, D. Scarano, G. Ricchiardi, A. Zecchina, Radially organized pillars of TiO_2 nanoparticles: synthesis, characterization and photocatalytic tests, J. Photochem. Photob. a-Chem., 242 (2012) 51-58.

[23] M.M. Rahman, F. Cesano, F. Bardelli, D. Scarano, A. Zecchina, Hybrid SnO_2/carbon composites: From foams to films by playing with the reaction conditions, Catal. Today, 150 (2010) 84-90.

[24] F. Cesano, S. Cravanzola, V. Brunella , D. Scarano, From polymer to magnetic porous carbon spheres: combined microscopy, spectroscopy and porosity studies, Frontiers in Materials, (2019, submitted).

[25] Q. Zhang, W. Wang, J. Goebl, Y. Yin, Self-templated synthesis of hollow nanostructures, Nanotoday, 4 (2009) 494-507.

[26] D. Prahas, Y. Kartika, N. Indraswati, S. Ismadji, Activated carbon from jackfruit peel waste by H_3PO_4 chemical activation: Pore structure and surface chemistry characterization, Chem. Eng. J., 140 (2008) 32-42.

[27] M.A. Lillo-Ròdenas, D. Cazorla-Amoròs, A. Linares-Solano, Understanding chemical reactions between carbons and NaOH and KOH: An insight into the chemical activation mechanism, Carbon, 41 (2003) 267–275.

[28] T.S. Tang Shu Hui, M.A.A. Zaini, Potassium hydroxide activation of activated carbon: a commentary Carbon Lett., 16 (2015) 275-280.

[29] B. Chang, Y. Wang, K. Pei, S. Yang, X. Dong, $ZnCl_2$-activated porous carbon spheres with high surface area and superior mesoporous structure as an efficient supercapacitor electrode, RSC Adv., 4 (2014) 40546.

[30] S. Ghosh, A.R. Barron, The effect of KOH concentration on chemical activation of porous carbon sorbents for carbon dioxide uptake and carbon dioxide–methane selectivity: the relative formation of micro- (<2 nm) versus meso- (>2 nm) porosity, Sustainable Energy Fuels, 1 (2017) 806.

[31] J. Wang, S. Kaskel, KOH activation of carbon-based materials for energy storage, J. Mater. Chem., 22 (2012) 23710.

[32] H. Xia, J. Wu, C. Srinivasakannan, J. Peng, L. Zhang, Effect of Activating Agent on the Preparation of Bamboo-Based High Surface Area Activated Carbon by Microwave Heating., High Temp. Mater. Proc., 35 (2015) 535-541.

[33] M. Molina-Sabio, F. Rodríguez-Reinoso, Role of chemical activation in the development of carbon porosity, Colloids Surf. A, 241 (2004) 15-25.

[34] A. Ahmadpour, B.A. King, D.D. Do, Comparison of Equilibria and Kinetics of High Surface Area Activated Carbon Produced from Different Precursors and by Different Chemical Treatments, Ind. Eng. Chem. Res., 37 (1998) 1329-1344.

[35] T.E. Rufford, D. Hulicova-Jurcakova, K. Khosla, Z. Zhu, G.Q. Lu, Microstructure and electrochemical double- layer capacitance of carbon electrodes prepared by zinc chloride activation of sugar cane bagasse, J. Power Sources, 195 (2010) 912-918.

[36] F. Cesano, M.M. Rahman, S. Bertarione, J.G. Vitillo, D. Scarano, A. Zecchina, Preparation and adsorption properties of activated porous carbons obtained using volatile zinc templating phases, Carbon, 50 (2012) 2047-2051.

[37] S. Yang, Y. Zhu, C. Cao, L. Peng, W.L. Queen, W. Song Controllable Synthesis of Multiheteroatoms Co-Doped Hierarchical Porous Carbon Spheres as an Ideal Catalysis Platform, Appl. Mater. Interfaces, 10 (2018) 19664–19672.

[38] A. Siyasukh, Y. Chimupala, N. Tonanon, Preparation of magnetic hierarchical porous carbon spheres with graphitic features for high methyl orange adsorption capacity, Carbon, 134 (2018) 207-221.

[39] D. Qiu, A. Gao, Z. Xie, L. Zheng, C. Kang, Y. Li, N. Guo, M. Li, F. Wang, R. Yang, Homologous Hierarchical Porous Hollow Carbon Spheres Anode and Bowls Cathode Enabling High-Energy Sodium-Ion Hybrid Capacitors Appl. Mater. Int., 10 (2018) 44483-44493.

[40] A.J. Romero-Anaya, M.A. Lillo-Ròdenas, A. Linares-Solano, Factors governing the adsorption of ethanol on spherical activated carbons, Carbon, 83 (2015) 240-249.

[41] J. Liu, N.P. Wickramaratne, S. Zhang Qiao, M. Jaroniec, Molecular-based design and emerging applications of nanoporous carbon spheres Nat. Mater., 14 (2015) 763-774.

[42] Q. Wang, X.-Y. Liang, R. Zhang, C.-J. Liu, X.-j. Liu, W.-M. Qiao, L. Zhan, L.-C. Ling, Preparation of polystyrene-based activated carbon spheres and their adsorption of dibenzothiophene, New Carbon Mater., 24 (2009) 55–60.

[43] Y. Sun, R. Chen, G. Zhao, F. Yang, Nanoindentation of carbon microspheres, Int. J. Mater. Res, 107 (2016) 687-691.

[44] C. Sarıcı-Ozdemir, Y. Onal, Synthesis of new activated carbons produced from polymer waste, Fuller. Nanotub. Car. N., 266 (2018) 451-457.

[45] A. Bazargan, C.W. Hui, G. McKay, Porous Carbons from Plastic Waste, Adv. Polym. Sci., 266 (2013).

[46] F. Cesano, M.M. Rahman, F. Bardelli, A. Damin, D. Scarano, Magnetic Hybrid Carbon via Graphitization of Polystyrene-co-Divinylbenzene: Morphology, Structure and Adsorption Properties., ChemistrySelect, 1 (2016) 2536–2541.

[47] J.M. Lee , M.E. Briggs, T. Hasell, A.I. Cooper, Hyperporous Carbons from Hypercrosslinked Polymers., Adv. Mater., 28 (2016) 9804-9810.

[48] H. Kaur, Polymer Resins as Nanoreactors for the Synthesis of Nanoparticles and Their Catalytic Application in C-C Coupling, pages 123-151, in: S. Sadjadi (Ed.) Encapsulated Catalysts, Academic Press2017, pp. 554.

[49] M. Thommes, K. Kaneko, A.V. Neimark, J.P. Olivier, F. Rodriguez-Reinoso, J. Rouquerol, K.S.W. Sing, Physisorption of gases, with special reference to the evaluation of surface area and pore size distribution (IUPAC Technical Report). Pure Appl. Chem., 87 (2015) 1051-1069.

[50] G. Lu, G.Q. Lu, Z.M. Xiao, Mechanical Properties of Porous Materials, J. P. Mat., 6 (1999) 359-368.